



HAL
open science

Sensitivity to the rheology and geometry of granular collapses by using the $\mu(I)$ rheology

Rudy Valette, Stéphanie Riber, Lucas Sardo, Romain Castellani, Frédéric Costes, Nathalie Vriend, Elie Hachem

► To cite this version:

Rudy Valette, Stéphanie Riber, Lucas Sardo, Romain Castellani, Frédéric Costes, et al.. Sensitivity to the rheology and geometry of granular collapses by using the $\mu(I)$ rheology. *Computers and Fluids*, 2019, 191, pp.104260. 10.1016/j.compfluid.2019.104260 . hal-02428724

HAL Id: hal-02428724

<https://hal.science/hal-02428724>

Submitted on 20 Dec 2021

HAL is a multi-disciplinary open access archive for the deposit and dissemination of scientific research documents, whether they are published or not. The documents may come from teaching and research institutions in France or abroad, or from public or private research centers.

L'archive ouverte pluridisciplinaire **HAL**, est destinée au dépôt et à la diffusion de documents scientifiques de niveau recherche, publiés ou non, émanant des établissements d'enseignement et de recherche français ou étrangers, des laboratoires publics ou privés.



Distributed under a Creative Commons Attribution - NonCommercial 4.0 International License

Sensitivity to the rheology and geometry of granular collapses by using the $\mu(I)$ rheology

Rudy Valette^a, Stéphanie Riber^a, Lucas Sardo^a,
Romain Castellani^a, Frédéric Costes^b, Nathalie Vriend^c
Elie Hachem^a,

^a*MINES ParisTech, PSL Research University, Centre de mise en forme des matériaux (CEMEF), CNRS UMR 7635, CS 10207 rue Claude Daunesse, 06904 Sophia-Antipolis, France.*

^b*Transvalor S.A., Parc de Haute Technologie, 694 Avenue du Dr. Maurice Donat, 06255 Mougins Cedex, France.*

^c*Department of Applied Mathematics and Theoretical Physics, University of Cambridge, Wilberforce Rd, Cambridge CB3 0WA, UK.*

Abstract

We introduce a numerical method for the 2D and 3D simulation of dense granular column collapses using the $\mu(I)$ inertial rheology. A sensitivity analysis of column deformation to the $\mu(I)$ model parameters is performed, showing that the inverse static friction parameter mostly controls the final deformation. Our computations show that the $\mu(I)$ inertial rheology is able to predict the different regimes of relative spreading as a function of aspect ratio a previously observed experimentally: a^1 , $a^{\simeq 0.66}$ and $a^{\simeq 0.5}$ scalings for, respectively, slumping for low aspect ratio, 2D and 3D spreading regimes for high aspect ratio. We show that the sublinear scalings for high aspect ratio spreadings are due to an extra dissipation at the impact of the falling

granular column. Finally we introduce the relative grain diameter as an additional dimensionless parameter that, for a fixed aspect ratio, increases the inertial number and then decreases the relative spreading.

Key words: finite element method, granular media, free surface

1 Introduction

Column collapses appear as a classical benchmark for studying granular flows. An initially cylindrical granular column of height h_i and radius r_i is released resulting in a flow driven by gravity. In this case, the aspect ratio a is defined as $a = h_i/r_i$.

For the last past years, several works focused on the dynamics of dry granular collapses. Lajeunesse et al. (2004) investigated initially axisymmetric granular collapses using glass beads and studied the influence of the aspect ratio a and the type of substrate (smooth or rough, rigid or erodible) on the final deposit radius r_f . They observed two different regimes of collapse depending on a : a slumping regime, where the column spreads through an avalanche of its flanks, for a lower than a critical aspect ratio a_c , and a spreading regime, where the whole column descends, for large a . They also observed that the sub-

Email addresses: `rudy.valette@mines-paristech.fr` (Rudy Valette),
`stephanie.riber@mines-paristech.fr` (Stéphanie Riber),
`lucas.sardo@mines-paristech.fr` (Lucas Sardo),
`romain.castellani@mines-paristech.fr` (Romain Castellani),
`frederic.costes@transvalor.com` (Frédéric Costes), `nv253@cam.ac.uk`
(Nathalie Vriend), `elie.hachem@mines-paristech.fr` (Elie Hachem).

strate does not affect significantly the granular dynamics and concluded that the aspect ratio is the main parameter driving granular collapses. Lube et al. (2004) also performed axisymmetric granular collapses using different granular materials (sand, sugar, salt, couscous, rice). They showed that the relative spreading $(r_f - r_i)/r_i$ scales as a^1 below a critical value of a close to 1.7 and scales as $a^{0.5}$ beyond. These two regimes (linear and sublinear) are consistent with, respectively, the slumping and spreading regimes observed by Lajeunesse et al. (2004). Lube et al. (2004) also showed a negligible influence of the type of grains on the collapse dynamics (i.e. relative spreading and time for emplacement), whereas Lajeunesse et al. (2004) demonstrated by geometrical arguments that the relative spreading should scale as $\simeq a/\mu$, μ being a macroscopic friction coefficient. Additionally, Balmforth and Kerswell (2005) showed a similar experimental trend. Lube et al. (2005) also performed two-dimensional granular collapses along a horizontal channel for different materials and concluded $r_f/r_i - 1$ scales as a^1 below a critical value of a close to 1.8, and scales as $a^{0.66}$ beyond, with no dependence on the type of material. Moreover all studies showed that the total time of motion scales as $(h_i/g)^{0.5}$, g being the gravitational acceleration.

Mangeney-Castelnau et al. (2004) and Larrieu et al. (2006) then proposed shallow-water models that allowed to retrieve the a^1 , $a^{\simeq 0.66}$ and $a^{\simeq 0.5}$ scalings for, respectively slumping, 2D and 3D spreading regimes, using a Coulombic friction model and adjustable parameters for basal friction. Recent progress (Andreotti et al., 2013) shows that dry granular flows dynamics is governed by a local dimensionless inertial number $I = \|\dot{\gamma}\| d/(\sqrt{p/\rho_f})$, as shown by Da Cruz et al. (2005) and then Jop et al. (2006), where $\|\dot{\gamma}\|$, d , p and ρ_f are, respectively, the norm of the strain rate tensor, the grains diameter, the

pressure and the grain material density.

The relevance of the local inertial approach has been proven using discrete granular collapse simulations by Lacaze and Kerswell (2009). Then, the so-called continuum $\mu(I)$ rheology model was first implemented in a numerical code for 2D collapses flows by Lagree et al. (2011). They compared with both analytical and discrete simulations, providing a conclusive validation of the implementation of this rheology for such flows. They also showed sensitivity plots for two $\mu(I)$ parameters. Furthermore, Ionescu et al. (2015) and Dunatunga and Kamrin (2015) performed additional validations of 2D flows for the $\mu(I)$ rheology, sensitivity analyses for 2D flows were also provided in Gesenhues et al. (2017) and 3D flows were computed by Gesenhues et al. (2018).

In this paper, 2D and 3D numerical simulations are presented for granular collapses using the $\mu(I)$ rheology, in order to provide a complete parameter sensitivity analysis and also check the relevance of this model in the 3D case. In the next section, the definition of the $\mu(I)$ rheology model is recalled as well as the present numerical strategy. Then, $\mu(I)$ parameter sensitivity analysis is performed for 2D and 3D granular collapses, followed by a discussion on energy partition during collapse, the role of grain diameter as an additional lengthscale, and the relevance of experimental mastercurves.

2 Constitutive equations and numerical strategy

2.1 The $\mu(I)$ rheology

The tensorial constitutive model of the $\mu(I)$ rheology is formulated such as in Jop et al. (2006):

$$\boldsymbol{\tau} = 2\mu(I)p \frac{\dot{\boldsymbol{\gamma}}}{\|\dot{\boldsymbol{\gamma}}\|}, \quad (1)$$

where $\boldsymbol{\tau}$ is the deviatoric part of the stress tensor, and $\mu(I)$ is the effective friction defined as:

$$\mu(I) = \mu_S + \frac{\mu_F - \mu_S}{\frac{I_0}{I} + 1}, \quad (2)$$

where μ_S , μ_F and I_0 represent respectively static friction coefficient, dynamic friction coefficient and a material constant that separates dense and collisional regimes.

Following Ionescu et al. (2015), the constitutive equations describing the $\mu(I)$ rheology may also be formulated as Bingham constitutive equations:

$$\begin{cases} \boldsymbol{\tau} = 2 \left(\eta_f(p, \|\dot{\boldsymbol{\gamma}}\|) + \frac{\tau_0(p)}{\|\dot{\boldsymbol{\gamma}}\|} \right) \dot{\boldsymbol{\gamma}} & \|\boldsymbol{\tau}\| > \tau_0(p), \\ \|\dot{\boldsymbol{\gamma}}\| = 0 & \|\boldsymbol{\tau}\| \leq \tau_0(p), \end{cases} \quad (3)$$

where $\tau_0(p)$ and $\eta_f(p, \|\dot{\boldsymbol{\gamma}}\|)$ represent the yield stress (pressure dependent) and the plastic viscosity (pressure and shear rate dependent) of the granular material. These quantities are defined as follows:

$$\tau_0(p) = \mu_s p, \quad (4)$$

$$\eta_f(p, \|\dot{\gamma}\|) = \frac{(\mu_F - \mu_s)p}{\sqrt{\frac{p}{\rho_f} \frac{I_0}{d} + \|\dot{\gamma}\|}}. \quad (5)$$

By analogy with Bingham flows, unyielded (quasi-static) regions correspond to a shear stress lower than $\mu_s p$.

2.2 Regularization method for $\mu(I)$ rheology flows

In this paper, granular flows are solved using a continuum approach, leading to the resolution of the following momentum and continuity equations:

$$\begin{cases} \rho (\partial_t \mathbf{v} + \mathbf{v} \cdot \nabla \mathbf{v}) + \nabla p - \nabla \cdot \boldsymbol{\tau} = \mathbf{f}, \\ \nabla \cdot \mathbf{v} = 0, \end{cases} \quad (6)$$

where \mathbf{v} is the velocity field, ∂_t is the time derivative, ∇ and $\nabla \cdot$ are gradient and divergence operators and \mathbf{f} is the gravity force $\rho \mathbf{g}$.

In the literature, two methods exist for coupling the $\mu(I)$ rheology with equations (6), namely (i) regularization methods, which consist in expressing the constitutive equations in terms of an effective viscosity; and (ii) exact methods, which consist in solving a minimization problem of the system energy using the Augmented Lagrangian method, leading to the exact computation of the stress field in unyielded regions. Chauchat and Medale (2013) introduced different regularization methods for $\mu(I)$ confined flows, while Lagree et al. (2011) used the simple regularization method for collapse flows. Alternatively, Ionescu et al. (2015) used an exact method for collapse flows and Lusso et al. (2017) showed recently that equivalent results are obtained with

the two methods. In this paper, a regularization method is chosen, owing to its algorithmic simplicity. More precisely, a Bercovier-Engelman regularization method was used, which consists in using a minimum shear rate $\|\dot{\gamma}\|_{min}$ as the regularization parameter. Moreover, the yield stress and plastic viscosity vanish as the pressure tends to zero, which may lead to unbounded values of the inertial number or vanishing viscosity. Thus, an additional regularization parameter is added, which corresponds to a minimum viscosity, taken as the air viscosity. The effective viscosity for the $\mu(I)$ formulation is finally:

$$\eta_{eff} = \max \left(\eta_{air}, \eta_f(p, \|\dot{\gamma}\|) + \frac{\tau_0(p)}{\sqrt{\|\dot{\gamma}\|^2 + \|\dot{\gamma}\|_{min}^2}} \right), \quad (7)$$

2.3 Numerical tools for the flow resolution

The numerical resolution of $\mu(I)$ rheology flows requires the resolution of mass and momentum equations 6, where the shear stress tensor $\boldsymbol{\tau}$ is defined as $\boldsymbol{\tau} = 2\eta_{eff}\dot{\boldsymbol{\gamma}}$, similarly to Riber et al. (2016). The momentum and mass equations are solved by using the Finite Element Method, and specifically using a Variational MultiScale method coupled with anisotropic mesh adaptation. Within a simple fixed point method, the viscosity term is computed using the final result of the VMS-Navier-Stokes solver (which means $\mathbf{v}_h + \mathbf{v}'$ and $p_h + p'$). For more details about the method, one can refer to Hachem et al. (2010) and Coupez and Hachem (2013).

This problem is described in an Eulerian framework, and considers both granular material and ambient fluid (air). Thus, a linear mixing law is used to consider properties of both fluids. A convective self-reinitializing Level-Set

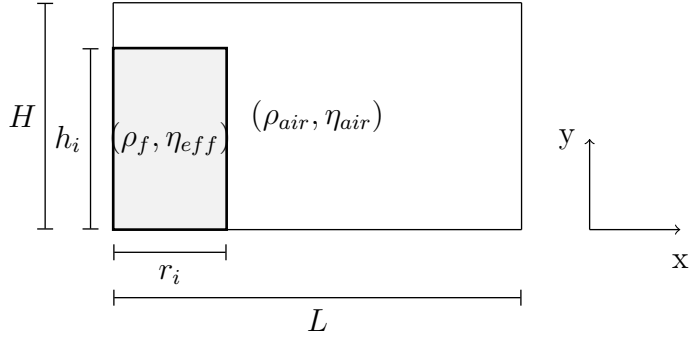


Fig. 1. Problem statement of the granular collapse problem

method (Khalloufi et al., 2016) was used to capture the interface position as a function of time. The resulting numerical framework allows to solve various free surface flow problems involving Bingham viscoplastic fluids (Valette et al., 2019a,b) and has been extended to the $\mu(I)$ rheology in this paper.

3 Two-dimensional numerical granular collapses

3.1 Problem statement

First, two-dimensional granular collapses were investigated. The geometry of the problem is illustrated in figure 1: a rectangular domain of length L and height H was filled with air, apart from a rectangular region set onto the bottom surface and filled with the granular material.

No-slip boundary conditions were applied at the bottom surface. However, the dynamic wetting of this surface by the granular material had to be ensured. To do so, perfect slip was imposed on the bottom surface in contact with air as well as in a small region downstream the front flow, which length was set to a few grains diameters (see figure 2). This length was also chosen for the

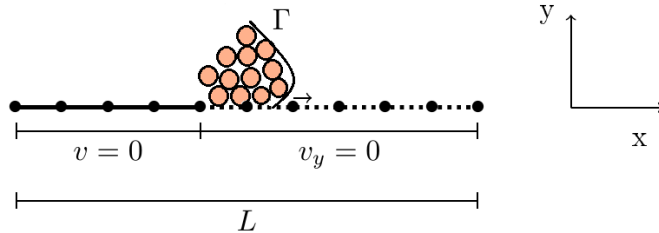


Fig. 2. Boundary conditions applied onto the bottom surface for two-dimensional granular collapses

minimum mesh size h_{min} in the computations.

3.2 Validation of the model

Validation of the present method was carried out by comparing results to those of Lagree et al. (2011), who performed two-dimensional granular collapses using the finite volume method and validated the model by comparing the obtained results with discrete simulations. These discrete simulations were set using grains of average diameter d , aspect ratio a and a total number of grains Nb_{grains} . To deduce an estimate for the height h_i and width r_i , we assumed a simple cubic volume and get $h_i = d\sqrt{aNb_{grains}}$ and $r_i = d\sqrt{Nb_{grains}/a}$. The continuous problem turns then into a dimensionless formulation as performed in Lagree et al. (2011): the characteristic length, velocity, time and density are taken respectively as h_i , $\sqrt{gh_i}$, $\sqrt{h_i/g}$ and ρ_f . In this new dimensionless problem, five dimensionless numbers control the system: the number of grains Nb_{grains} , the initial aspect ratio of the column a , and the dimensionless rheological parameters μ_S , $\Delta\mu$ and I_0 .

Consequently, the inertial number computation involves the dimensionless grain diameter $\bar{d} = 1/\sqrt{aNb_{grains}}$ and granular density $\bar{\rho}_f = 1$. The dimension-

less geometries become: initial column radius $\bar{r}_i = 1/a$, initial column height $\bar{h}_i = 1$.

By considering dimensionless shear rate and pressure fields, the inertial number can be rewritten as:

$$I = \frac{\|\bar{\dot{\gamma}}\|}{\sqrt{\bar{p}aNb_{grains}}}, \quad (8)$$

where $\bar{p} = p/\rho gh_i$.

Three granular collapses with different aspect ratios $a = 0.5, 1.42$ and 6.26 were tested, respectively with $Nb_{grains} = 3407, 6041$ and 6036 . The same rheological parameters as Lagree et al. (2011) were considered: $\mu_S = 0.32$, $\Delta\mu = 0.28$ and $I_0 = 0.4$. The regularization parameters were taken as $\|\bar{\dot{\gamma}}\|_{min} = 10^{-3}$ and $\bar{\eta}_{air} = 10^{-4}$. The mesh was dynamically adapted according to the effective viscosity, velocity norm and Level-Set fields, as described in Riber et al. (2016), and the number of elements was constrained to $\simeq 4 \cdot 10^4$.

Figures 3.(a), 3.(b) and 3.(c) illustrate the height profiles at different instants, $\bar{t} = 0, 1, 2$ and 4 respectively. For $a = 0.5$ (figure 3.(a)), we observed that the granular deposit corresponds to a truncated cone, leading to a maximum height on the left wall (equal to 1). For $a = 1.42$ (figure 3.(b)), a larger spreading was observed, leading to the granular collapse on the left side. Thus, the run-out distance was larger as a increased, leading to a wide final deposit (figure 3.(c) for $a = 6.26$).

Figures 4.(a), 4.(b) and 4.(c) illustrate the dimensionless front position according to the dimensionless time, and compare the obtained results with the

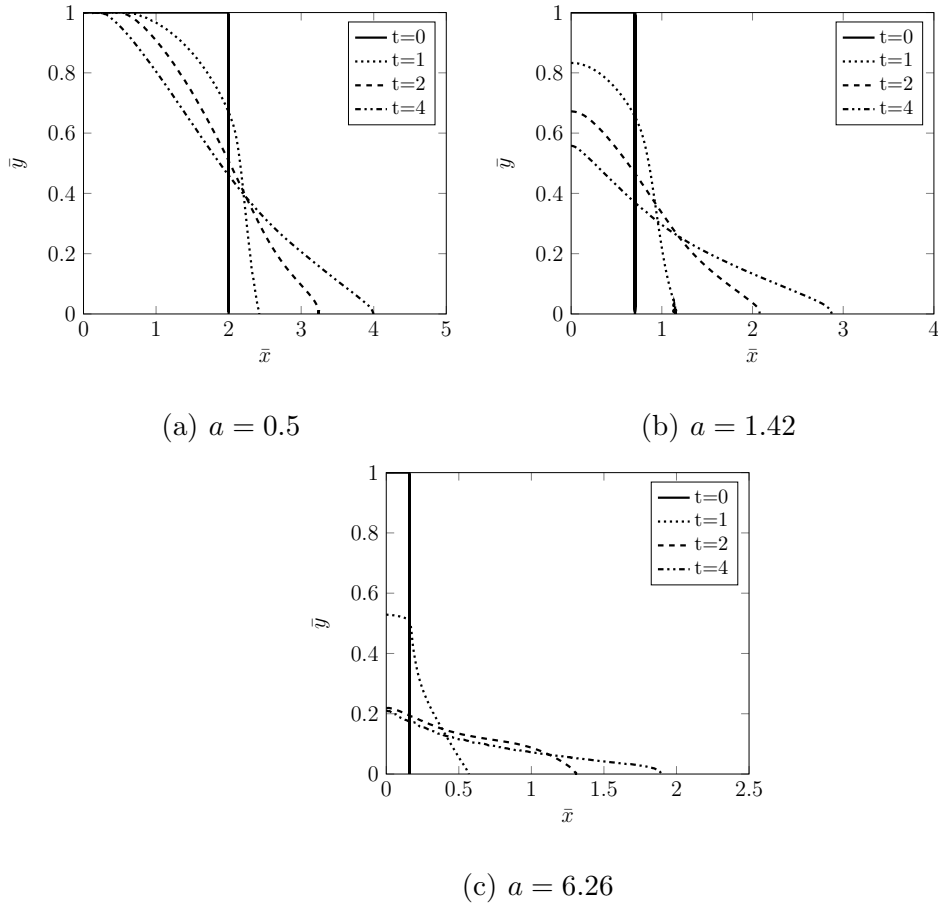


Fig. 3. Height profiles after granular collapses with different aspect ratios (for (a) $a = 0.5$; (b) $a = 1.42$; (c) $a = 6.26$) at several instants $\bar{t} = 0, 1, 2$ and 4

ones of Lagree et al. (2011). It is observed that our simulations got closer to the discrete simulations, than the continuum method of Lagree et al. (2011), probably due to improved accuracy with mesh adaptation.

3.3 Flow sensitivity to the $\mu(I)$ parameters

In this section, the influence of $\mu(I)$ parameters ($\mu_S, \Delta\mu, I_0$) is analyzed. Different numerical collapses were performed by using materials with different rheologies. Two different column geometries were studied: one column collapse corresponding to the linear regime ($a = 1.42$), and one corresponding to the

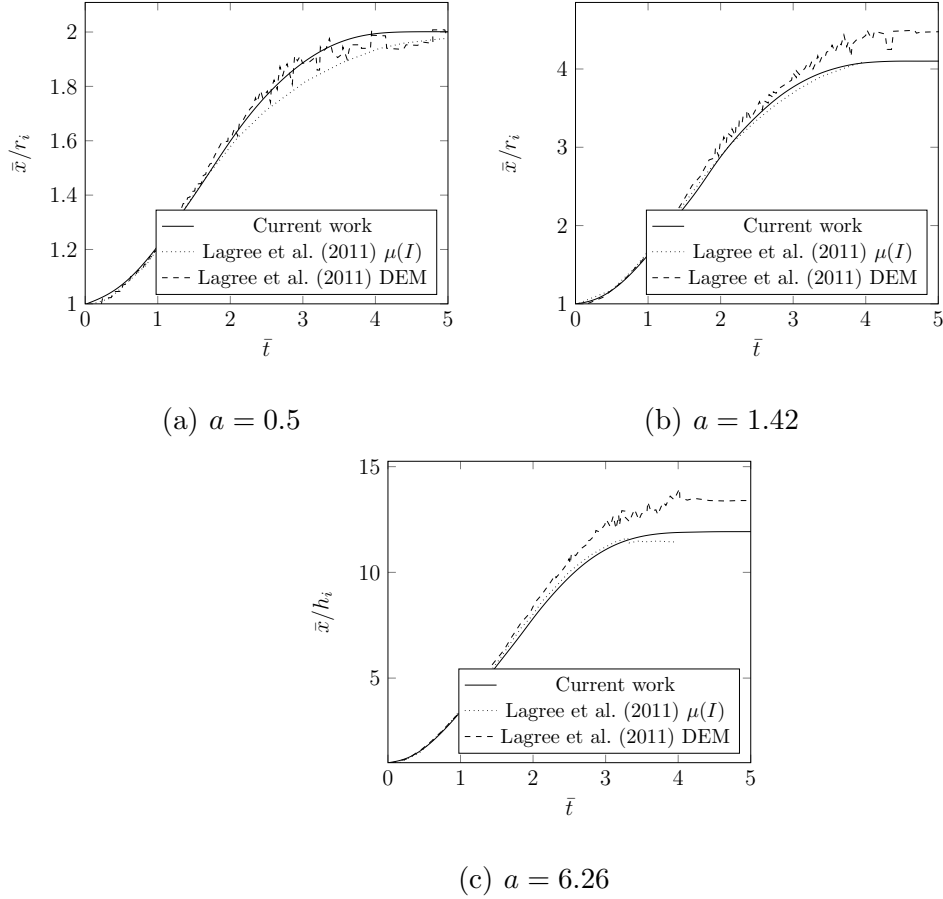


Fig. 4. Dimensionless position of the front according to dimensionless time for granular collapses with different aspect ratios ($a = 0.5, 1.42$ and 6.26)

power-law regime ($a = 10$).

3.3.1 Sensitivity to the static friction coefficient

First, the influence of μ_S was studied. Four collapses with different μ_S were performed: $\mu_S = 0.32, 0.42, 0.52$ and 0.62 . Figure 5 illustrates the final deposit. It was observed that static friction coefficient changes drastically the final shape of the flow. Indeed, from $\mu_S = 0.52$ to 0.62 , the run-out distance is 20% larger.

The same analysis have been performed with a granular collapse with larger a

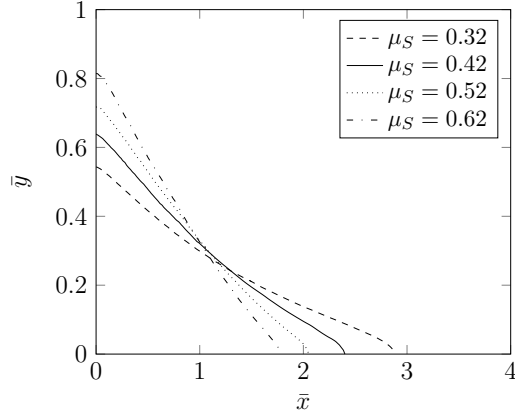


Fig. 5. Final profiles after granular collapses ($a = 1.42$) with different μ_S

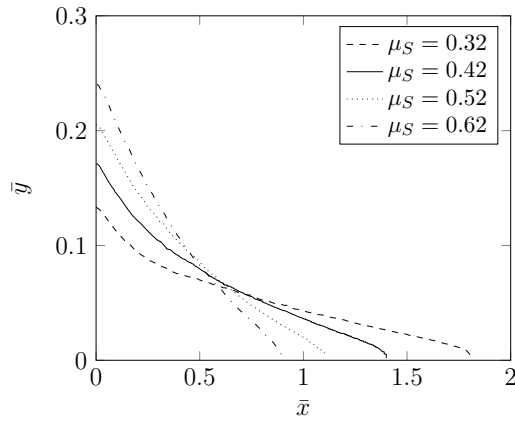


Fig. 6. Final profiles after a granular column ($a = 10$) with different μ_S

($a = 10$), illustrated in figure 6, leading to the same conclusion that the static friction coefficient has a strong influence on the run-out distance.

Figure 7 illustrates the run-out distance dependence to μ_S for the two columns geometries. It is observed that the run-out distance follows a power-law curve with respect to μ_S . The exponent is found close to -1.2 for both flows, which is consistent with the scaling obtained by Lajeunesse et al. (2004).

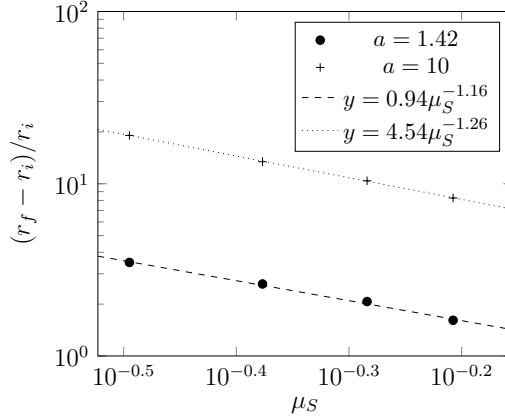


Fig. 7. Run-out distance of the flow with respect to the static friction coefficient

3.3.2 Sensitivity to the dynamic friction coefficient

Then, the influence of μ_F was analyzed. Granular collapses with different $\Delta\mu$ ($\Delta\mu = \mu_F - \mu_S$) were performed and run-out distances were compared. In these simulations, μ_S was fixed to 0.32. Figure 8 illustrates the final granular profiles after the collapse. It was observed that the final height measured on the symmetry plane was independent of μ_F and remained constant. However, a difference was noticed on the run-out distance, which increased as μ_F decreased. Such a behavior was expected, as the inertial number is large in the vicinity of the front flow.

The evolution of the front position during the simulation (figure 9) shows that only the deceleration stage depends on μ_F . By analyzing curves 8 and 9, μ_F acts at the end of the flow, by elongating (low μ_F) the final granular profile, while keeping the maximum height constant.

Then, the same analysis were performed for a granular collapse with higher a ($a = 10$, figure 10). The same conclusion as for lower a , was established.

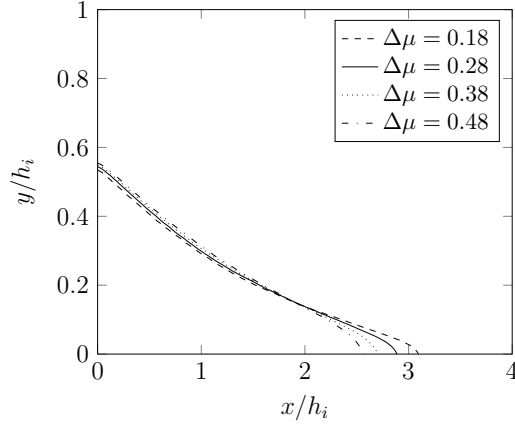


Fig. 8. Final profiles after granular collapses with $a = 1.42$ and $\Delta\mu = 0.18, 0.28, 0.38$ and 0.48

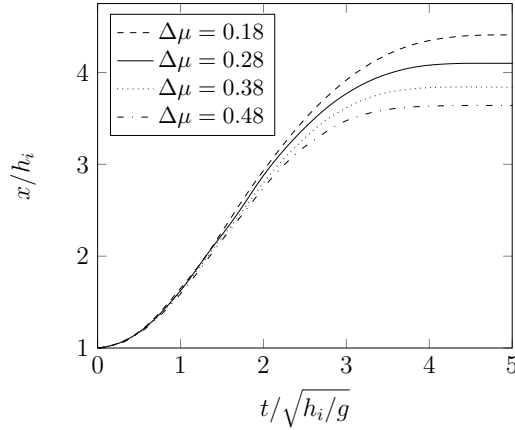


Fig. 9. Dimensionless position of the front with respect to dimensionless time after granular collapses with $a = 1.42$ and $\Delta\mu = 0.18, 0.28, 0.38$ and 0.48

Finally, figure 11 illustrates dimensionless run-out of the granular flow with respect to $\Delta\mu$, for two granular collapses with $a = 1.42$ and 10 . It was observed that the dimensionless run-out distance also follows a power-law curve in the vicinity of the chosen set of parameters and that $\Delta\mu$ had a stronger relative impact on the run-out distance for low a . However, the influence of $\Delta\mu$ on the run-out distance remains lower than the one for μ_S .

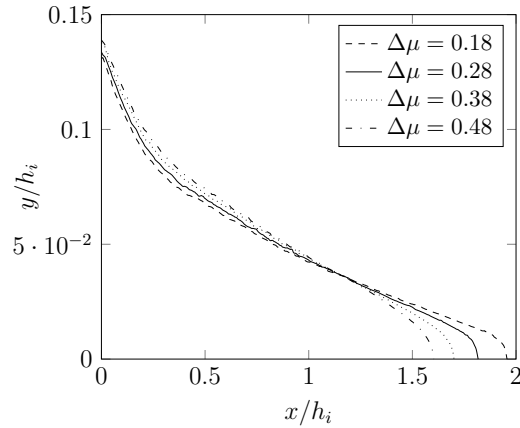


Fig. 10. Final profiles after a granular collapse ($a = 10$) for different $\Delta\mu$

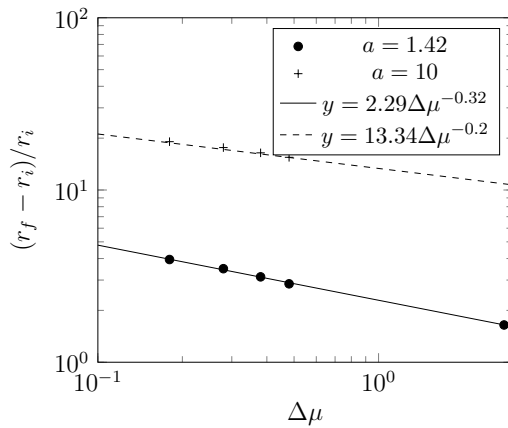


Fig. 11. Dimensionless run-out distance with respect to $\Delta\mu$

3.3.3 Sensitivity to I_0

Finally, the influence of I_0 was analyzed. Three granular collapses with different I_0 (0.04, 0.4 and 4) were performed. Figure 12 shows the evolution of the dimensionless front position during the collapse. It was observed that the flow spreads further for large I_0 granular collapses, which is an expected behaviour. Indeed, low I_0 leads to a fast transition between quasi-static and dense regimes, which induces smaller unyielded regions.

Figure 13 illustrates the dimensionless run-out distance with respect to I_0 ,

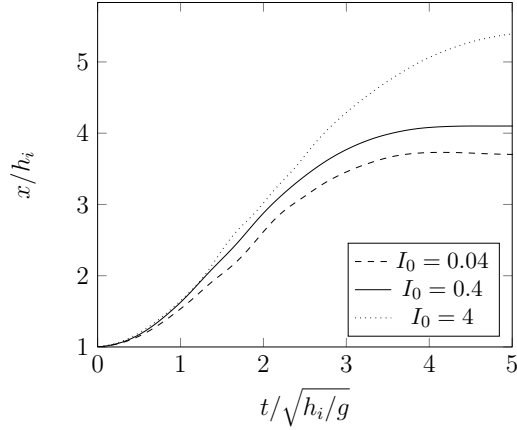


Fig. 12. Dimensionless front position with respect to the dimensionless time after granular collapses with $a = 1.42$ and $I_0 = 0.04, 0.4$ and 4

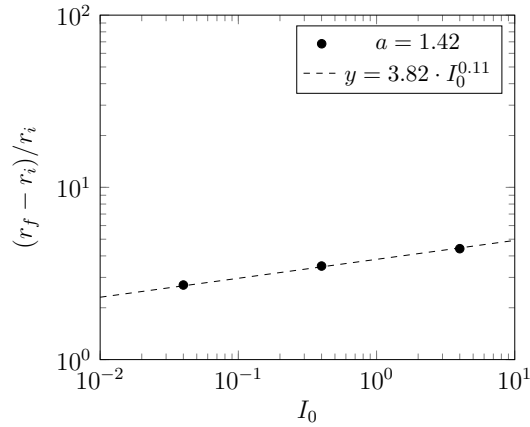


Fig. 13. Dimensionless run-out distance according to I_0

which follows a power-law curve of exponent 0.11, meaning that I_0 has a small influence on the granular dynamics for the chosen set of parameters. Let us notice that the influence of I_0 should be high for large aspect ratios flows as such flows would become more inertial, this point is discussed in a later paragraph.

In conclusion, two-dimensional granular collapses with granular materials having different $\mu(I)$ parameters were performed. The analysis of each parameter shows that the predominant physical parameter impacting the final run-out

distance is μ_S . It was observed that μ_F has also a small influence (approximately four times less than μ_S), particularly during the deceleration stage. Finally, I_0 has a small influence compared to μ_S , for low h_i .

3.4 Flow sensitivity to the geometry

3.4.1 Granular regimes according to the aspect ratio

The flow sensitivity to the initial column geometry was also investigated. Figure 14 shows the normalized flow front position according to the aspect ratio a . As obtained in Lube et al. (2005), a linear curve was found for low a (lower than $a_c \approx 7$). Moreover, a power-law curve with exponent 0.7 was found for large a (larger than $a_c \approx 7$):

$$\frac{r_f - r_i}{r_i} \approx \begin{cases} 1.72 & a^{0.97} \quad a \leq 7 \\ 2.96 & a^{0.69} \quad a \geq 7 \end{cases} \quad (9)$$

These results are consistent with the ones obtained by Lagree et al. (2011), namely a limit between linear and power-law regimes $a_c \approx 7$, and a power-law exponent of 0.7. In the experimental work conducted by Lube et al. (2005), the same type of curves were found. They determined, however, a power-law exponent of 2/3 and a much lower critical aspect ratio. This difference could be explained by the choice of the numerical rheological parameters (μ_S typically) and maybe by additional physics missing in the present model, typically thin layer/non-local effects as indicated by GDR MiDi (2004).

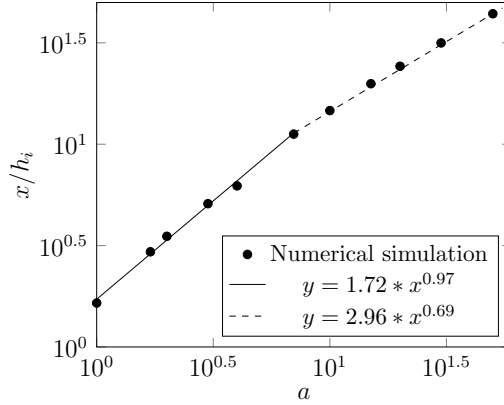


Fig. 14. Dimensionless run-out distance with respect to a after two-dimensional granular collapses

3.4.2 Energy analysis

In order to explain the two observed power-law regimes, we propose to confirm the theory proposed by Larrieu et al. (2006), who suggested that, for large enough a , some more of the (vertical) kinetic energy of the fall is dissipated when the grains impact on the base, therefore not converted into horizontal kinetic energy.

Figures 15, 16 and 17 show relative (with respect to initial potential energy) energy partition (kinetic, potential, mechanical and dissipated energies) during granular collapse for, respectively, aspect ratio $a = 1.42$, $a = 10$ and $a = 50$. As expected, both the kinetic energy and final dissipated energy increase with aspect ratio. For low aspect ratio, one notices that the maximum kinetic energy was reached at a time $t \simeq \sqrt{2h_i/g}$, which is the impact time for a free fall from h_i , but most of exchange of energy comes from potential to dissipated energies. For large aspect ratios, the maximum kinetic energy is much larger, is reached earlier, then decreases quickly until $t \simeq \sqrt{2h_i/g}$, while the dissipated energy jumps suddenly.

This result suggests that the extra-dissipation for large aspect ratio indeed occurs during the impact, which is confirmed on figures 18, 19 and 20, which show the volume fraction of flowing regions (non-zero velocity) during a collapse for, respectively, $a = 1.42$, $a = 10$ and $a = 50$. Indeed, the graphs show that for large a , nearly the whole volume was flowing, including the bottom center region, confirming the measured extra dissipation. Figure 21 shows the height profiles formed during a granular column collapse with $a = 50$, plotted for different times. At the free fall time $t \simeq 1.5\sqrt{h_i/g}$, a crater and a crest were formed, creating a wave that was advected away for the subsequent times, and then spread away at late times, the crest being damped in the inner direction. This complex flow is divided in dense and inertial regions, forming respectively the top and bottom of the advected wave, as shown on figure 22.

3.5 *Flow features close to arrest*

3.5.1 *Time of flow arrest*

It is well known that regularization methods do not ensure a strict flow stop at long times, but rather a slow creep. Consequently a method to measure precisely the flow arrest time was introduced. One expects to find the time for the flow stop when the stress is smaller than μ_{sp} everywhere in the flow domain. However, as the pressure depends on the flow geometry, there exist some regions (typically close to the free surface) where μ_{sp} is arbitrary small. Consequently, in these regions, the effective viscosity tends to the regularized

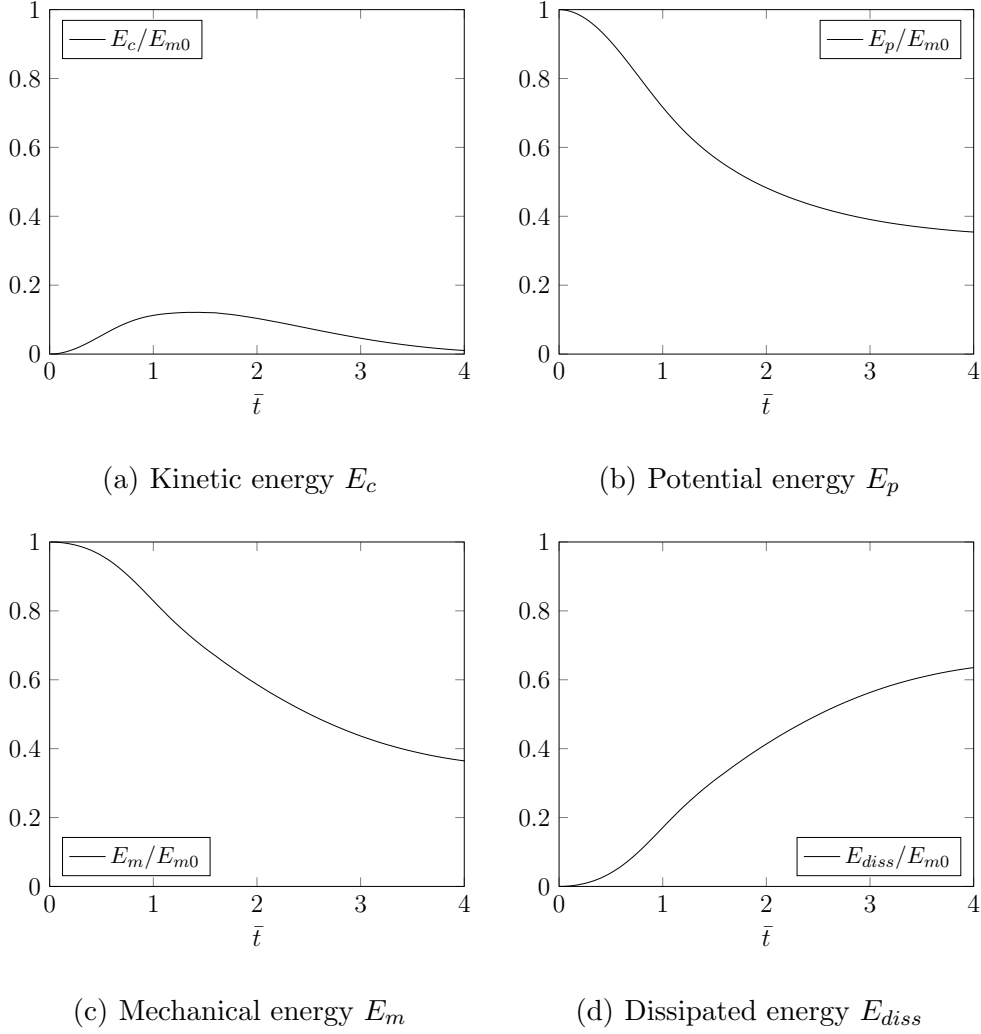


Fig. 15. Relative energy partition during a granular collapse with $a = 1.42$

value η_{min} , whereas stress close to the surface could occur from potential (for slow flows) or kinetic (for fast flows) energy. For example, we noticed that the front flow did not satisfy the stress criterion in the two last elements, due to the present numerical treatment of triple point/line movement. However, when plotting the mean shear rate $\int_{\Omega_f} \|\bar{\dot{\gamma}}\| \Omega_f$ at different instants (see figure 23) we noticed that it increased at early times, corresponding to the flow start, then reached a maximum, followed by a plateau. Finally, the mean shear rate decreased suddenly down to a finite plateau value, scaling inversely with η_{min} . We then chose the corresponding time as the flow stop time.

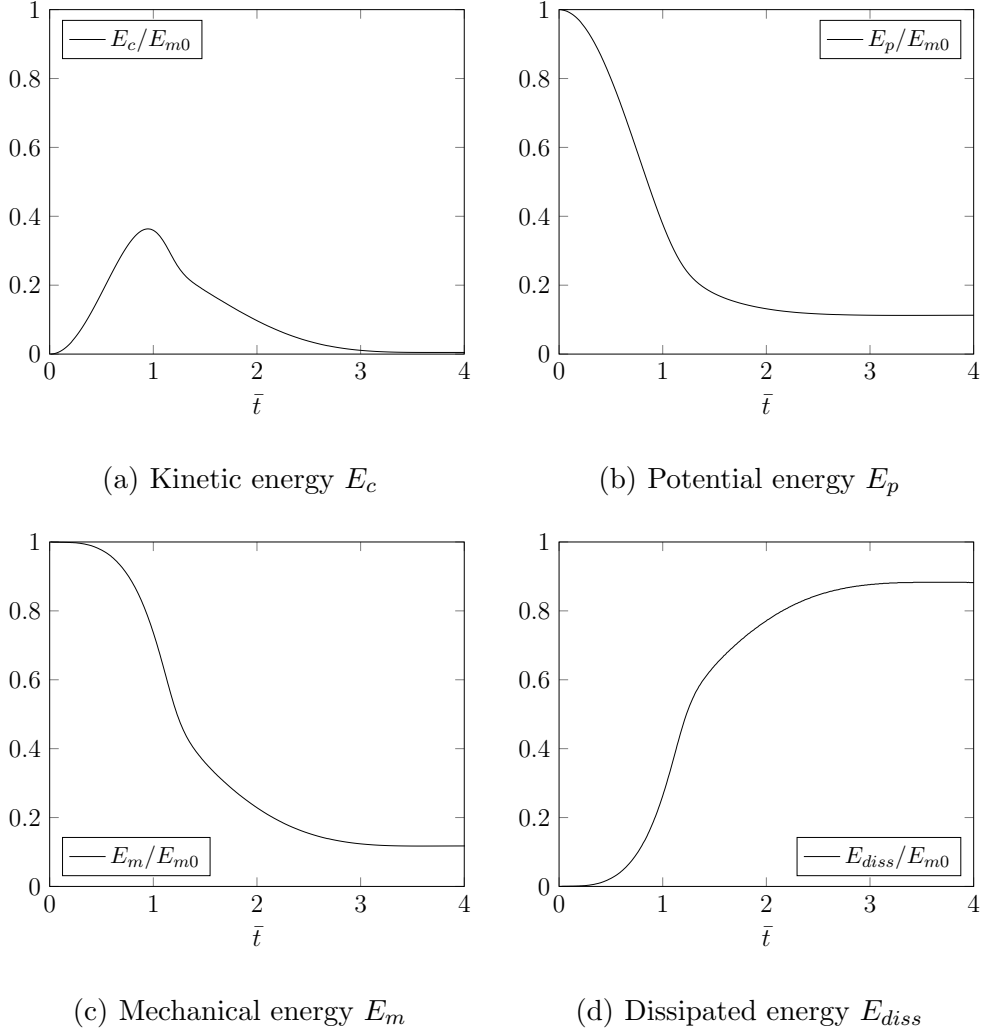
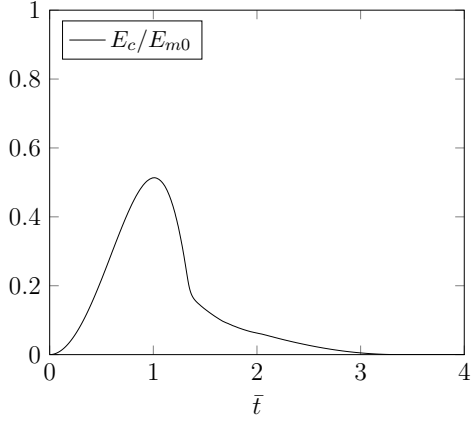


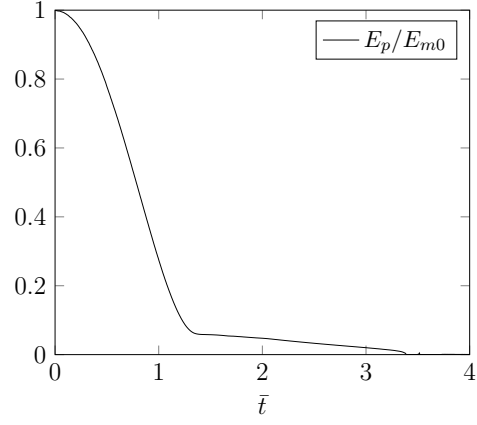
Fig. 16. Relative energy partition during a granular collapse with $a = 10$

3.5.2 Sensitivity to $\mu(I)$ parameters

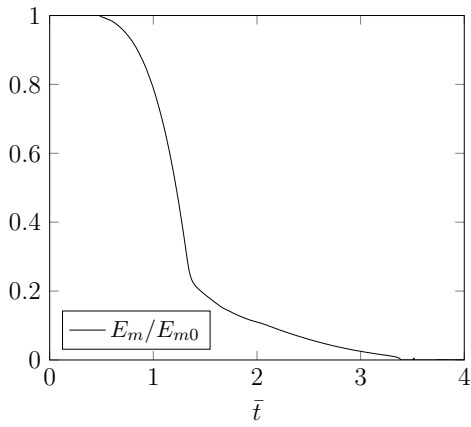
For the same collapse, it was observed that the arrest time of the flow depends strongly on μ_S : the higher μ_S , the earlier the flow arrest, and the lower the run-out distance (see figure 24.a). Moreover, it was observed that $\Delta\mu$ had a smaller influence: the larger $\Delta\mu$, the sooner the flow arrest, and the lower the run-out distance (see figure 24.b). For larger aspect ratios, the arrest time was much less dependent on rheology, as the global flow duration scaled as the free fall time.



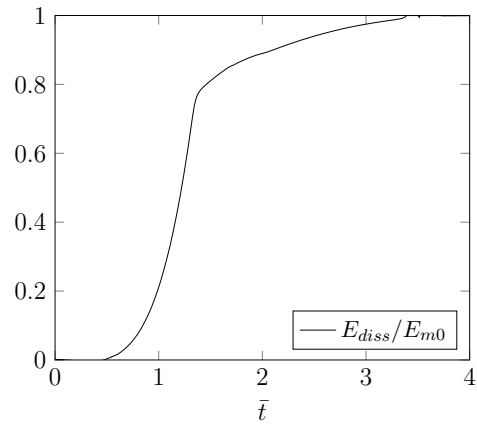
(a) Kinetic energy E_c



(b) Potential energy E_p



(c) Mechanical energy E_m



(d) Dissipated energy E_{diss}

Fig. 17. Relative energy partition during a granular collapse with $a = 50$

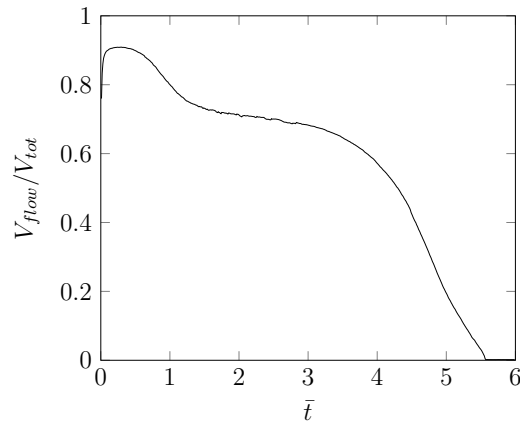


Fig. 18. Volume fraction of flowing regions (non zero velocity) during a collapse with $a = 1.42$

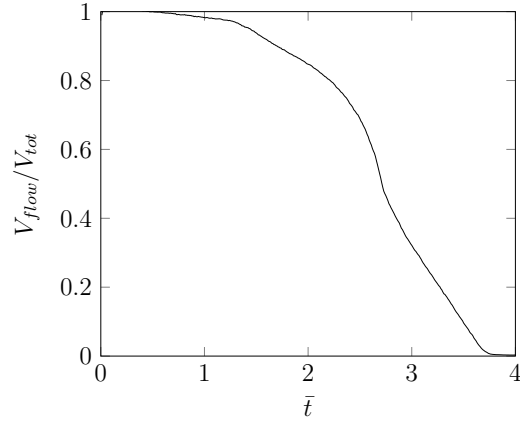


Fig. 19. Volume fraction of flowing regions (non zero velocity) during a collapse with $a = 10$

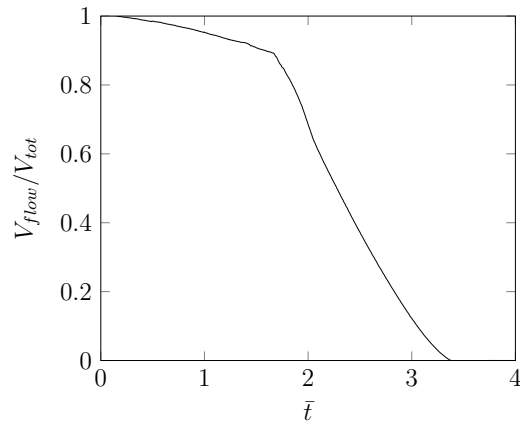


Fig. 20. Volume fraction of flowing regions (non-zero velocity) during a collapse with $a = 50$

3.5.3 Sensitivity to the aspect ratio

When varying the aspect ratio from small to large, according to the transition value a_c , we observed two types of flow arrests. First, for small aspect ratio, the flow consisted of a first expansion of the edges, that stopped before the global arrest, followed by a rearrangement of the surface, close to the symmetry plane (see shear rates plots on figure 25). For large aspect ratio, the flow spreaded from the edges until the arrest (see figure 26), because the kinetic energy was

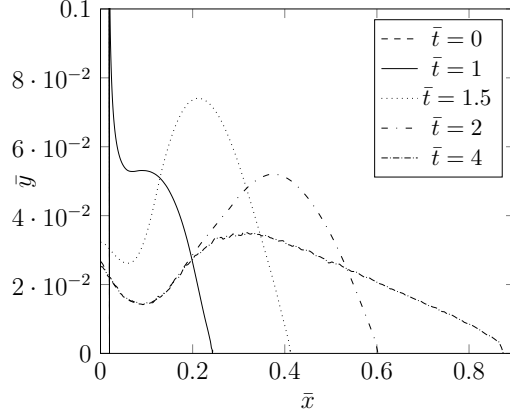


Fig. 21. Height profiles during a granular column collapse with $a = 50$, plotted for different non-dimensional times $\bar{t} = t/\sqrt{h_i/g}$

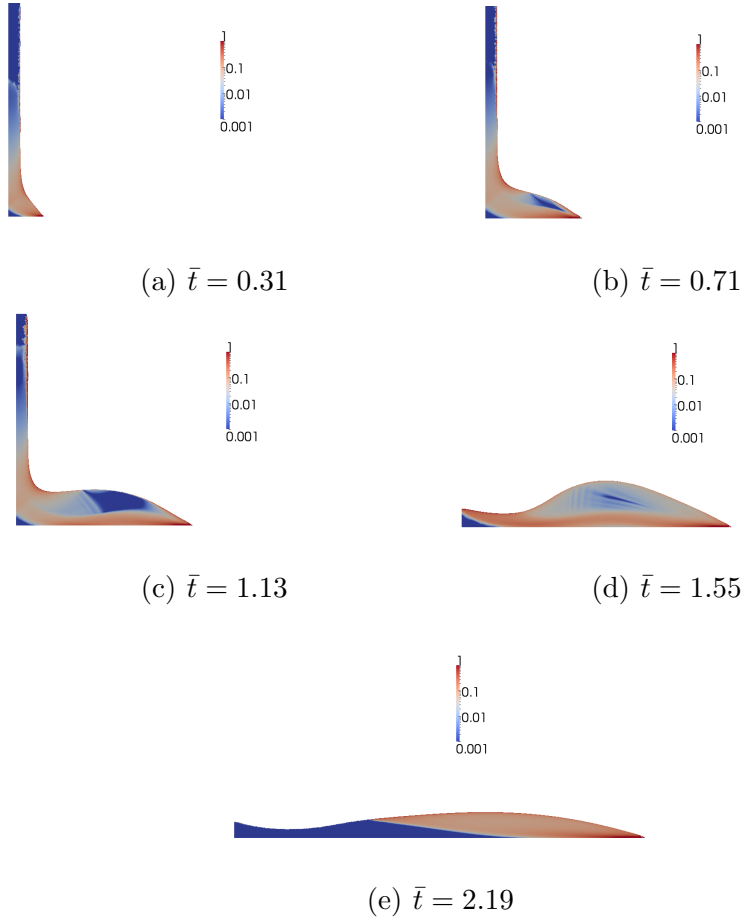


Fig. 22. Dense vs. inertial regions for different non-dimensional times $\bar{t} = t/\sqrt{h_i/g}$, plotted as I/I_0 for a granular collapse with $a = 50$. Color bar is the shear rate field $\bar{\gamma}$.

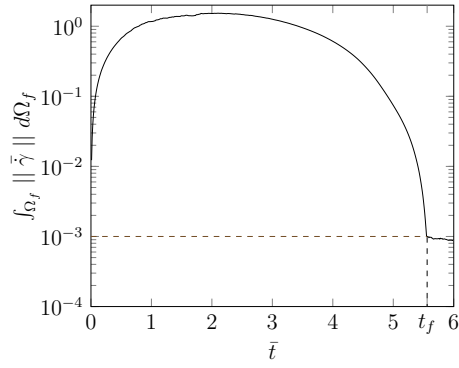


Fig. 23. Evolution of mean shear rate during a granular collapse with $a = 1.42$

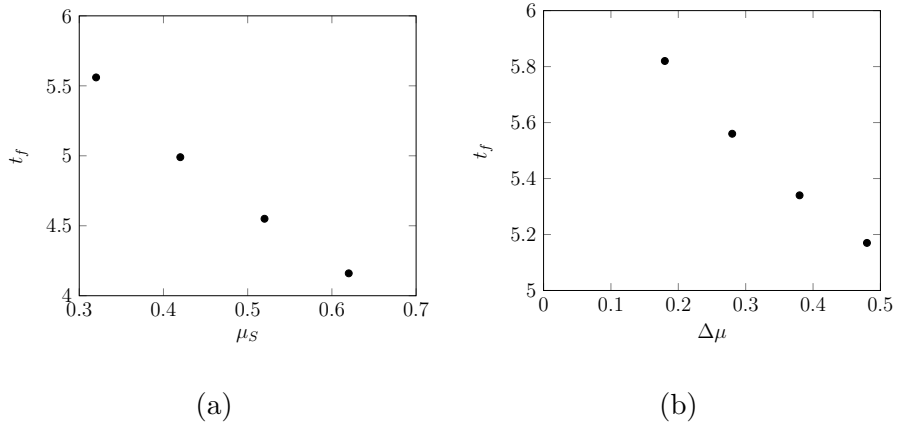


Fig. 24. Variation of arrest time with rheological constants: (a) Influence of μ_S ; (b) Influence of $\Delta\mu$

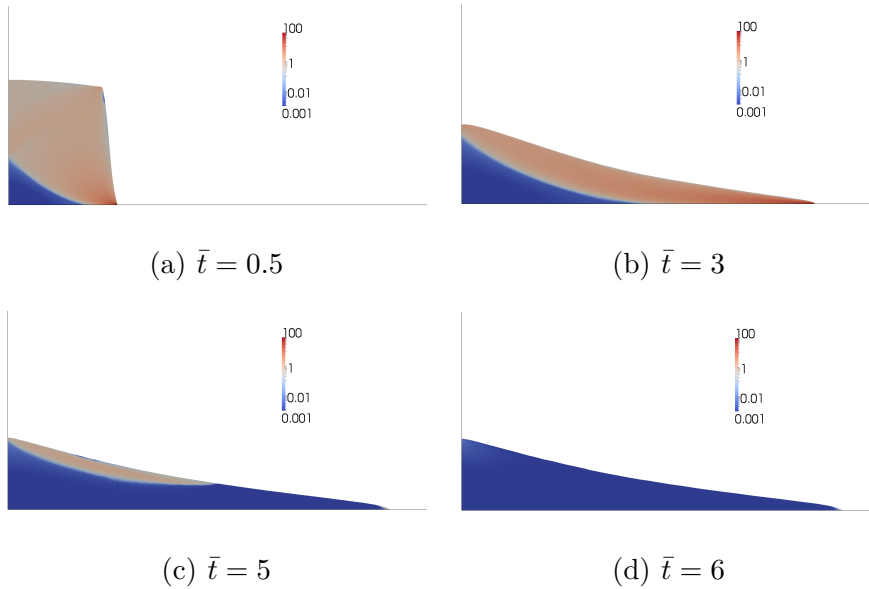


Fig. 25. Shear rate for a granular collapse with $a = 1.42$ plotted at several instants

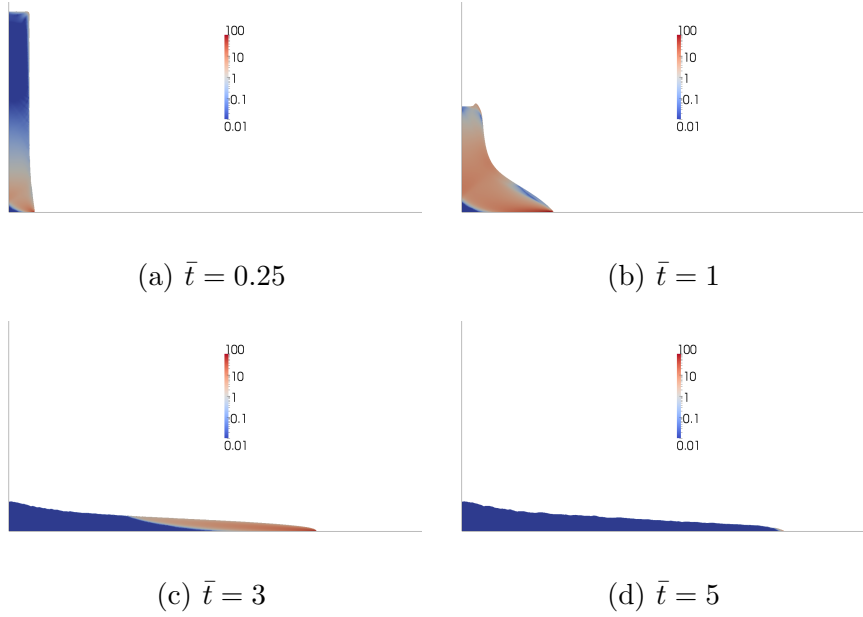


Fig. 26. Shear rate during a granular collapse with $a = 10$, plotted at several instants

concentrated in the front flow.

3.6 Master curves for granular collapses

As introduced at the beginning of this paper, Lube et al. (2005) pointed that for any rheology and geometrical features, the flow follows a same curve, representing the relative run-out distance $(r - r_i)/(r_f - r_i)$ according to the relative time \bar{t}/t_f , where r_f is the total spreading time.

Figure 27 illustrates this curve for granular collapses ($a = 10$) computed with the present method, for different values of μ_S . It was observed that the run-out distance follows a curve nearly independent of μ_S , where only slight differences were observed, particularly, a slower acceleration phase for larger μ_S .

Figure 28 illustrates the same curve for granular collapses computed for different $\Delta\mu$. This analysis showed that $\Delta\mu$ had an even smaller influence on the

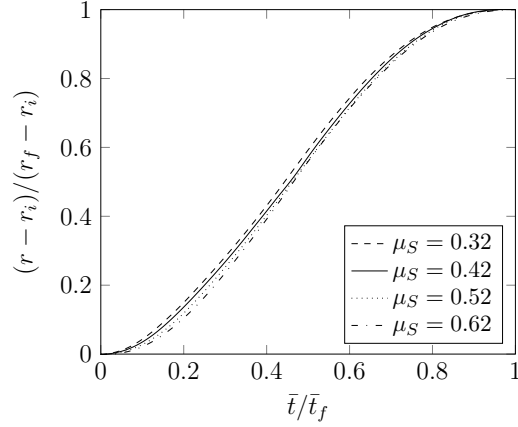


Fig. 27. Run-out distance according to dimensionless time for granular collapses for $a = 10$ with different μ_S

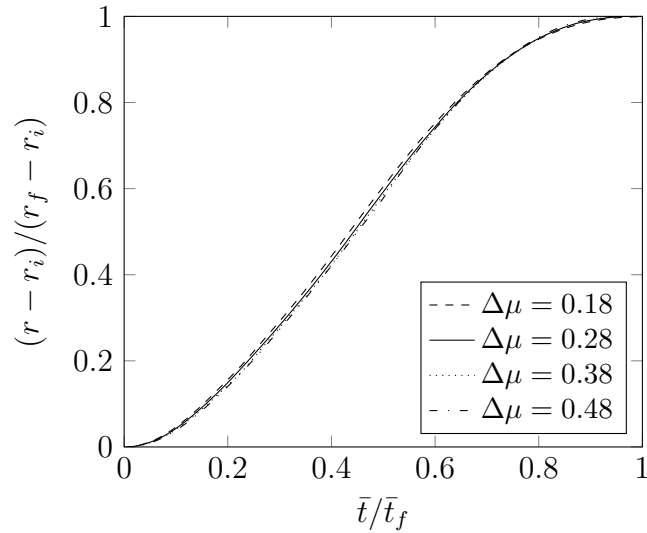


Fig. 28. Run-out distance with respect to dimensionless time for granular collapses for $a = 10$ with different $\Delta\mu$

relative granular dynamics.

Lube et al. (2005) outlined that reduced granular dynamics is independent of geometrical and rheological flow features, by demonstrating that granular materials follow a same curve (relative run-out distance according to relative time). Several granular collapses computations were tested using different μ_S

and $\Delta\mu$, as illustrated in curves 27 and 28. The present results suggest, according to the $\mu(I)$ theory, that rheological constants have a weak influence on the reduced granular dynamics, confirming Lube et al. (2005) results. Alternatively, it could be concluded that the materials used in Lube et al. (2005) were not rheologically different, as suggested by Balmforth and Kerswell (2005).

3.7 Conclusion

In this section, two-dimensional granular collapses computations were performed with materials exhibiting different rheological features, and also for different aspect ratios a . First, multiphase $\mu(I)$ rheology flows have been validated with results of Lagree et al. (2011) obtained with discrete methods (DEM). Then, the influence of rheological features has been analyzed. It has been shown that μ_S is the dominant rheological parameter that drives the spreading.

Then, the influence of a has been studied. The two regimes observed in Lube et al. (2005) have been found: a linear regime for low a , and a power-law one for high a . Moreover, it was found that the $\mu(I)$ model can predict a quasi universal relative time-distance curve.

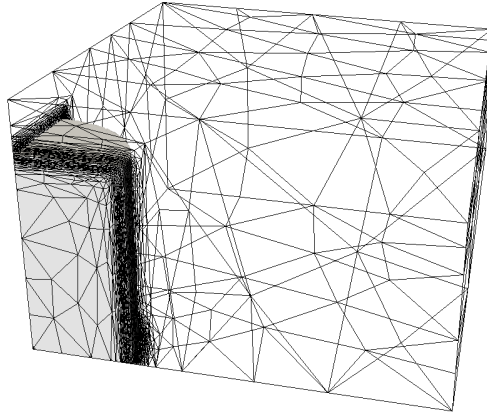


Fig. 29. Initial granular column and adaptive mesh of a three-dimensional granular collapse simulation

4 Three-dimensional granular collapses

4.1 Problem statement

The present model was extended to three-dimensional granular collapses. The geometry of the problem is illustrated in figure 29. A cylindrical granular column with initial height h_i and radius r_i was considered. The computations were performed in a rectangular domain (with two symmetry planes) of height H in z direction and length L in both x and y directions.

Symmetry conditions were applied on the two lateral surfaces. The pressure was set to zero on the other surfaces except at the bottom surface, where no-slip conditions were applied. As detailed in the previous section, one needed to set slip zones downstream the flow front, fixed to a few grains diameter.

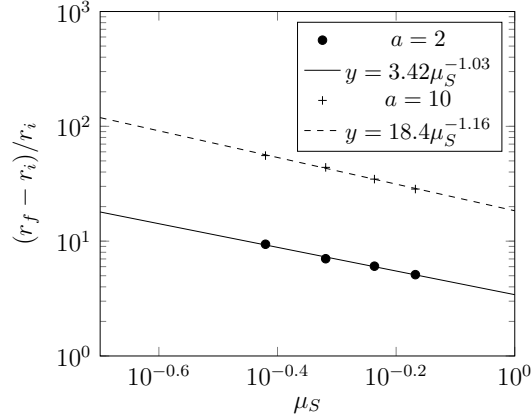


Fig. 30. Dimensionless final run-out distance square according to μ_S for three-dimensional collapses

4.2 Flow sensitivity to $\mu(I)$ parameters

In this part, the influence of $\mu(I)$ parameters on the final run-out distance was analyzed. Figure 30 illustrates the dimensionless final run-out squared distance according to μ_S . The obtained curve follows a power-law regime with exponent ≈ -1 according to μ_S . Indeed, $(r_f^2 - r_i^2)/r_i^2$ is a global measure of deformation which, at first order, is expected to scale as $1/\mu_S$. Let us notice that, in 2D, the equivalent global measure of deformation is the run-out distance $(r_f - r_i)/r_i$.

Figure 31 illustrates dimensionless final run-out distance square according to $\Delta\mu$. As observed for two-dimensional granular collapses, the granular material spreads further when $\Delta\mu$ is lower. Moreover, it is observed that the curve follows a power-law with exponent ≈ -1 . Thus, as for two-dimensional granular collapses, μ_S has a stronger influence (three times more) than μ_F .

Finally, figure 32 illustrates dimensionless run-out distance square according to I_0 . As observed for two-dimensional granular collapses, the granular material

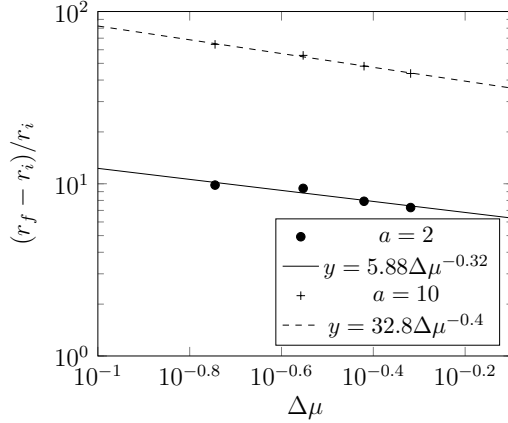


Fig. 31. Dimensionless run-out distance square according to $\Delta\mu$ for three-dimensional granular collapses

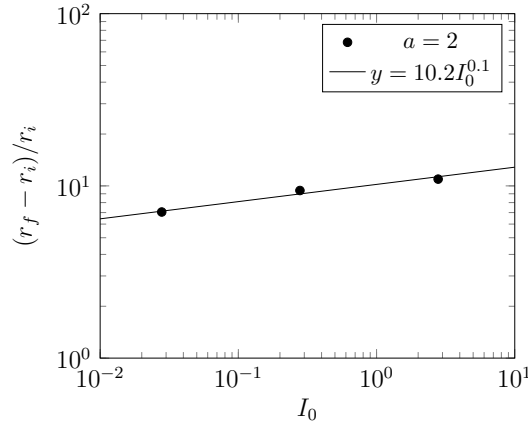


Fig. 32. Dimensionless run-out distance square according to I_0 for three-dimensional collapses

spreads further when I_0 is lower. Moreover, it is observed that the curve follows a power-law with exponent 0.1 on I_0 . As for the 2D case, influence of I_0 is small compared to the one of μ_S (ten times smaller), at least for the chosen set of parameters.

Consequently, three-dimensional simulations of the $\mu(I)$ rheology show that material constant sensitivities are similar to the two-dimensional cases when considering global measures of deformation.

4.3 Influence of the aspect ratio

Three-dimensional granular collapses with different a were then performed, using $\mu(I)$ parameters from Jop et al. (2006): $\mu_S = 0.38$, $\Delta\mu = 0.28$, $I_0 = 0.279$, $\rho_f = 2500 \text{ kg} \cdot \text{m}^{-3}$ and $d = 0.54 \text{ mm}$.

Figure 33 illustrates the dimensionless position of the final front according to a . It was observed that for large aspect ratios ($a > 2.7$), the granular dynamics followed a power-law curve with exponent 0.54. For low aspect ratios ($a < 2.7$), a linear regime was found, similarly to two-dimensional granular collapses. Thus, the critical aspect ratio has been found equal to $a_c \approx 2.7$:

$$\frac{r_f - r_i}{r_i} = \begin{cases} 1.2a & a < 2.7 \\ 1.93a^{0.54} & a > 2.7 \end{cases} \quad (10)$$

Consequently, three-dimensional simulations show that the $\mu(I)$ rheology is able to retrieve experimental exponents measured by Lube et al. (2004) and Lajeunesse et al. (2004).

4.4 Grain diameter as an additional lengthscale

With the inertial number being defined as $I = || \dot{\gamma} || d / (\sqrt{p/\rho_f})$, the grain diameter d acts as an additional lengthscale for fixed aspect ratio a . The global velocity, strain rate and pressure scaling as, respectively, $\sqrt{(h_i)}$, $1/\sqrt{(h_i)}$ and h_i , the inertial number then scales as $d/h_i = d/(ar_i)$. One then expects, for fixed d and a , a larger effective friction for low r_i , and consequently a less

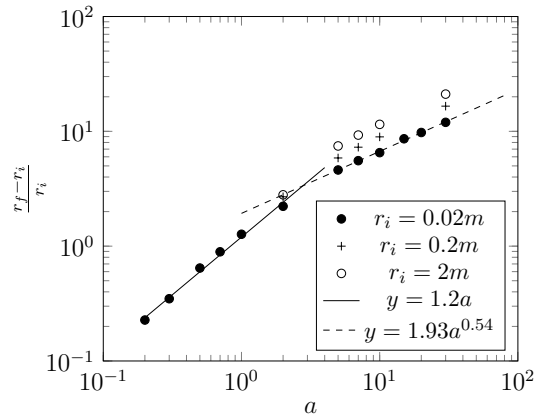


Fig. 33. Dimensionless final run-out distance according to a after three-dimensional granular collapses and influence of h_i

efficient spreading.

Figure 33 illustrates this statement, by comparing granular collapses at various a for $r_i = 0.2m$ and $r_i = 0.02m$, with the grain diameter being fixed to $d = 0.54mm$. The relative spreading was indeed lower for large values of d/r_i . This behaviour is consistent with the dimensional analysis performed by Lagree et al. (2011), who pointed out that the total number of grains (here, the number of grains per unit height) is a control dimensionless parameter for the flow.

5 Conclusion

In this paper, two and three-dimensional numerical simulations of granular collapses have been performed, using the $\mu(I)$ inertial rheology. In the experimental literature of Lube et al. (2004), it was observed that the granular rheology does not influence the flow dynamics, which was in contradiction with Balmforth and Kerswell (2005), which asserted that the friction coef-

ficient plays an important role in the flow dynamics (better spreading for low frictional materials). The numerical simulations performed in this paper showed that the inverse static friction coefficient μ_S mostly controls the relative deformation of the column. The role of dynamic friction coefficient and characteristic inertial number I_0 are of second order.

Our computations show that the $\mu(I)$ inertial rheology is able to predict the different regimes of relative spreading as a function of aspect ratio a previously observed for 2D and 3D experimental collapses: a^1 , $a^{\simeq 0.66}$ and $a^{\simeq 0.5}$ scalings for, respectively, slumping for low aspect ratio, 2D and 3D spreading regimes for large aspect ratio. We have also shown that the sublinear scalings for high aspect ratio spreadings are due to an extra dissipation at the impact of the falling granular column. Finally we have introduced the relative grain diameter as an additional dimensionless parameter that, for a fixed aspect ratio, increases the inertial number and then decreases the relative spreading. This influence of grain diameter vs. initial radius will be experimentally investigated in a future work.

Acknowledgements

S.R. would like to acknowledge support from the FUI COMCEPT project, R.V. would like to thank P.-Y. Lagr e, S. Luding, O. Pouliquen and P. Saramito for fruitful discussions.

References

- Andreotti, B., Forterre, Y., Pouliquen, O., 2013. Granular media: from liquid to solid. Cambridge University Press.
- Balmforth, N., Kerswell, R., 2005. Granular collapse in two dimensions. *J. Fluid Mech* 538, 399–428.
- Chauchat, J., Medale, M., 2013. A three-dimensional numerical model for dense granular flows based on the $\mu(i)$ rheology. *J. Comput. Phys.* 256, 696–712.
- Coupez, T., Hachem, E., 2013. Solution of high-reynolds incompressible flow with stabilized finite element and adaptive anisotropic meshing. *Comput. Meth. Appl. Mech. Engn* 267, 65–85.
- Da Cruz, F., Emam, S., Prochnow, M.e.a., 2005. Rheophysics of dense granular materials: Discrete simulation of plane shear flows. *Phys. Rev. E* 72.
- Dunatunga, S., Kamrin, K., 2015. Continuum modeling and simulation of granular flows through their many phases. *J. Fluid Mech* .
- GDR MiDi, 2004. On dense granular flows. *Eur. Phys. J. E* 14, 341–365.
- Gesenhues, L., Camata, J., Côrtes, A., Rochinha, F., Coutinho, A., 2018. Finite element simulation of complex dense granular flows using a well-posed regularization of the $\mu(i)$ -rheology. submitted to *Comput. Fluids* .
- Gesenhues, L., Camata, J., Coutinho, A., 2017. Simulation of a column collapse for dense granular flows. doi:10.20906/CPS/CILAMCE2017-0778.
- Hachem, E., Rivaux, B., Kloczko, T., Digonnet, H., Coupez, T., 2010. Stabilized finite element method for incompressible flows with high reynolds number. *J. Comput. Phys.* 229, 8643–8665.
- Ionescu, I., Mangeney, A., Bouchut, F., Roche, O., 2015. Viscoplastic modeling of granular column collapse with pressure-dependent rheology. *J. Non-Newt.*

- Fluid Mech. 219, 1–18.
- Jop, P., Pouliquen, O., Forterre, Y., 2006. A constitutive law for dense granular flows. *Nature* 441, 727–730.
- Khallowfi, M., Mesri, Y., Valette, R., Massoni, E., Hachem, E., 2016. High fidelity anisotropic adaptive variational multiscale method for multiphase flows with surface tension. *Comput. Meth. Appl. Mech. Engrn* 307, 44–67.
- Lacaze, L., Kerswell, R., 2009. Axisymmetric granular collapse : a transient 3d flow test of visco-plasticity. *Phys. Rev. Letters* 102.
- Lagree, P.Y., Staron, L., Popinet, S., 2011. The granular column collapse as a continuum : validity of a two-dimensional navier-stokes model with a $\mu(i)$ rheology. *J. Fluid Mech* , 1–31.
- Lajeunesse, E., Mangeney-Castelnau, A., Vilotte, J., 2004. Spreading of a granular mass on a horizontal plane. *Phys. Fluids* 16.
- Larrieu, E., Staron, L., Hinch, E.J., 2006. Raining into shallow water as a description of the collapse of a column of grains. *J. Fluid Mech* 554, 259–270.
- Lube, G., Huppert, H., Stephen, R., Sparks, J., Hallworth, M., 2004. Axisymmetric collapses of granular columns. *J. Fluid Mech* 508, 175–199.
- Lube, G., Huppert, H.E., Sparks, R., Freundt, A., 2005. Collapses of two-dimensional granular columns. *Phys. Rev.* 72.
- Lusso, C., Ern, A., Bouchut, F., Mangeney, A., Farin, M., Roche, O., 2017. Two-dimensional simulation by regularization of free surface viscoplastic flows with drucker-parger yield stress and application to granular collapse. *J. of Comp. Phys.* 333, 387–408.
- Mangeney-Castelnau, A., Bouchut, F., Lajeunesse, E., Aubertin, A., Vilotte, J., Pirulli, M., 2004. On the use of saint-venant equations for simulating the spreading of granular mass. *J. Geophys. Res.* 199, 177–215.

- Riber, S., Valette, R., Mesri, Y., Hachem, E., 2016. Adaptive variational multiscale method for bingham flows. *Comput. Fluids* 138, 51–60.
- Valette, R., Hachem, E., Khalloufi, M., Pereira, A., Mackley, M., Butler, S., 2019a. The effect of viscosity, yield stress, and surface tension on the deformation and breakup profiles of fluid filaments stretched at very high velocities. *J. Non-Newt. Fluid Mech.* 263, 130–139.
- Valette, R., Riber, S., Pereira, A., Khalloufi, M., Sardo, L., Hachem, E., 2019b. Adaptive finite element framework for simulating two and three-dimensional viscoplastic free surface flows. submitted to *J. Non-Newt. Fluid Mech.* .